Translational Oncology
www.transonc.com

Volume 6 Number 4 August 2013 pp. 493–503 493

Tumor Dynamics in Response to Antiangiogenic Therapy with Oral Metronomic Topotecan and Pazopanib in Neuroblastoma Xenografts[1]

Sushil Kumar*,†, Reza Bayat Mokhtari†,‡, Indhira Dias Oliveira§, Syed Islam‡, Silvia Regina Caminada Toledo§, Herman Yeger†,‡ and Sylvain Baruchel*,†

*Division of Hematology and Oncology, Department of Pediatrics, The Hospital for Sick Children, Toronto, Ontario, Canada; †Institute of Medical Science, University of Toronto, Toronto, Ontario, Canada; ‡Department of Pediatric Laboratory Medicine, The Hospital for Sick Children, Toronto, Ontario, Canada; §Oncology Section, Department of Pediatrics and Division of Genetics, Department of Morphology and Genetics, Federal University of São Paulo, São Paulo, Brazil

Abstract

Metronomic chemotherapy, combined with targeted antiangiogenic drugs, has demonstrated significant anticancer efficacy in various studies. Though, tumors do acquire resistance. Here, we have investigated the effect of prolonged therapy with oral metronomic topotecan and pazopanib on tumor behavior in a neuroblastoma mouse xenograft model. SK-N-BE(2) xenograft–bearing mice were treated with either of the following regimens (daily, orally): vehicle (control), 150 mg/kg pazopanib, 1.0 mg/kg topotecan, and combination of topotecan and pazopanib. Planned durations of treatment for each regimen were 28, 56, and 80 days or until the end point, after which animals were sacrificed. We found that only combination-treated animals survived until 80 days. Combination halted tumor growth for up to 50 days, after which gradual growth was observed. Unlike single agents, all three durations of combination significantly lowered microvessel densities compared to the control. However, the tumors treated with the combination for 56 and 80 days had higher pericyte coverage compared to control and those treated for 28 days. The proliferative and mitotic indices of combination-treated tumors were higher after 28 days of treatment and comparable after 56 days and 80 days of treatment compared to control. Immunohistochemistry, Western blot, and real-time polymerase chain reaction revealed that combination treatment increased the hypoxia and angiogenic expression. Immunohistochemistry for Glut-1 and hexokinase II expression revealed a metabolic switch toward elevated glycolysis in the combination-treated tumors. We conclude that prolonged combination therapy with metronomic topotecan and pazopanib demonstrates sustained antiangiogenic activity but also incurs resistance potentially mediated by elevated glycolysis.

Translational Oncology (2013) 6, 493–503

Introduction

There has been significant improvement in the survival rate among pediatric cancer patients since the 1970s. In neuroblastoma, the 5-year survival rate in children older than 1 year has increased from 35.3% in 1975 to 1978 to 64.8% in 1999 to 2002 [1]. However, the survival rate in high-risk and recurrent neuroblastoma is still less than 40% [2]. Drug resistance and dose-limiting toxicities are the major causes of therapy failure in neuroblastoma; therefore, newer strategies like

Address all correspondence to: Dr Sylvain Baruchel, New Agent and Innovative Therapy Program, The Hospital for Sick Children, 555 University Ave, Room 9418, Black Wing, Toronto, Ontario M5G 1X8, Canada. E-mail: sylvain.baruchel@sickkids.ca

[1]The PhD program of S.K. was supported by a Queen Elizabeth II/Dr Dina Gordon Malkin Scholarship in Science and Technology (2011/12) and by the James Fund for Neuroblastoma Research.

Received 15 March 2013; Revised 24 May 2013; Accepted 28 May 2013

DOI 10.1593/tlo.13286

antiangiogenic therapy are being explored to enhance patient survival with advanced neuroblastoma.

Antiangiogenic therapy has opened up new avenues and therapeutic options in the field of cancer chemotherapy. Among several possible antiangiogenic strategies for pediatric cancers, low-dose metronomic (LDM) chemotherapy and targeted antiangiogenic agents have gained widespread attention [3,4]. Single agents have demonstrated significant efficacy in various clinical and preclinical settings [5,6]. Apart from antiangiogenesis, LDM chemotherapy acts by several other mechanisms. Metronomic cyclophosphamide and temozolomide have demonstrated antitumor immune stimulation by inhibiting anti-immune T regulatory cells [7]. Topotecan has shown an antitumor immune response of T cells in experimental gliomas [8]. Vascular endothelial growth factor (VEGF) receptor inhibitors sunitinib and sorefenib have also depleted T regulatory cells and immunosuppressive myeloid-derived suppressor cells in renal cell carcinoma (RCC) patients [9]. However, as single modalities LDM therapy and antiangiogenic drugs have limited efficacy [4]. Enhanced antitumor efficacies have been achieved by combining these two therapies. A combination of LDM chemotherapy and a VEGF pathway targeting antiangiogenic agent was first reported with metronomic vinblastine combined with anti–VEGF receptor 2 antibody DC101 in neuroblastoma models [10]. More recent examples of such preclinical investigations are LDM gemcitabine + sunitinib (pancreatic cancer), LDM cyclophosphamide + thrombospondin (colon cancer), LDM cyclophosphamide + endostar (lung cancer), and LDM topotecan + sunitinib and bevacizumab (neuroblastoma) [11–14]. Such combinations have demonstrated clinical efficacy in various adult and pediatric cancers [15–21]. These examples also include the pediatric clinical trials conducted by us, which involves the combination of metronomic chemotherapy with repositioned drug celecoxib, owing to the antiangiogenic property of COX2 inhibitors [19,20].

Combining LDM topotecan and pazopanib has also demonstrated significant advantage over either single agent alone in ovarian cancer preclinical models [22,23]. Encouraged by these positive preclinical observations, we investigated the efficacy of LDM topotecan and pazopanib in mouse xenograft models of pediatric solid tumors [24]. Recently, this combination has shown advantage over the single agents in colon cancer preclinical model [6]. Phase I trial of this combination in gynecologic tumors has been conducted [25]. However, one disadvantage with the combination is that, even though it delayed tumor growth, it failed to stop tumor growth in mice models of colon cancer, ovarian cancer, and neuroblastoma even during the therapy. In our neuroblastoma metastatic model, the combination therapy significantly enhanced survival, but animals eventually succumbed to the increasing tumor burden [24].

Our observations are in line with the report that metronomic chemotherapy and antiangiogenic agents, even in combination with chemotherapeutics, have not produced any significant enhancement in overall survival [26–30]. Cancers either remain refractory to the maintenance regimen of antiangiogenic therapy or show recurrence or relapse. Therefore, there is a need to understand the changes in tumor behavior in response to prolonged antiangiogenic therapy.

With this in mind, we have attempted to gain insight into the dynamics of tumor response to LDM topotecan (TP) and pazopanib (PZ) in our neuroblastoma mouse xenograft models. In the present study, we evaluated the tumor behavior and phenotypic alterations after treatment with LDM topotecan and pazopanib, over time, *in vivo* using an MYCN-amplified cell line. Our results show that the vascular supply initially reduced by the combination treatment underwent a maturation process by developing a pericyte coverage leading to continued growth and the potential to grow in the hypoxic environment. Thus, tumors appear to adapt and acquire renewed vigor.

Materials and Methods

Drugs and Reagents

Topotecan, (*S*)-10-[(dimethylamino)methyl]-4-ethyl-4,9-dihydroxy-1*H*-yrano [3′,4′:6,7] indolizino[1,2-*b*] quinoline-3,14 (4*H*,12*H*)-dione monohydrochloride, and pazopanib, (5-[[4-[(2,3-Dimethyl-2H-indazol-6-yl)methyl amino]-2-pyrimidinyl]amino]-2-methylbenzolsulfonamide, were provided by GlaxoSmithKline (Collegeville, PA). SK-N-BE(2) cell line was obtained from American Type Culture Collection (Manassas, VA). The positive control tissue for hexokinase II (HK-II; glioblastoma) was provided by Dr Gelareh Zadeh (The Hospital for Sick Children, Toronto, Ontario). All other positive control tissues were provided by the Division of Pathology, Department of Pediatric Laboratory Medicine, The Hospital for Sick Children.

Tumor Treatment

The preclinical SK-N-BE(2) neuroblastoma xenograft model has been previously described [24]. SK-N-BE(2) cells (1×10^6) were implanted in the subcutaneous abdominal fat pad of non-obese diabetic immunodeficient mice/severely combined immunodeficient (NOD/SCID) mice (4-8 weeks), and when the tumors reached ≈0.5 cm in diameter, mice were randomized into four treatment groups: control (untreated), $n = 4$; PZ (150 mg of pazopanib), $n = 8$; TP (1.0 mg/kg topotecan), $n = 8$; TP + PZ (combination of topotecan and pazopanib, same doses as single agents), $n = 12$. Durations of treatment planned for each regimen were 28, 56, and 80 days with end points for TP and PZ not expected to go beyond 56 days, as per our observation in the previous study [24]. Therefore, the mice in control, TP, PZ, and TP + PZ were subrandomized into one, two, and three subgroups, respectively ($n = 4$ in each subgroup). In any subgroup, all four mice were sacrificed on the same day, either on completion of assigned duration of treatment or when one animal in that subgroup reached the end point, whichever occurred first. The criteria for end point termination were either tumor size exceeding 2.0 cm in diameter or animals showing signs of morbidity.

Immunohistochemistry

Harvested tumors were either fixed in 10% formalin or rapidly frozen in OCT media. Formalin-fixed and paraffin-embedded tissue sections were cut at 5 to 7 μm, deparaffinized by xylene and ethanol, and rehydrated in phosphate-buffered saline (PBS; #311-010-CL; Wisent Bioproducts, St Bruno, Quebec, Canada). Following antigen retrieval with citrate buffer (pH 6.0), sections were blocked for 1 hour in 2% BSA. Sections were subsequently incubated with primary antibodies. The primary antibodies were anti–phosphohistone H3 (PH3; Millipore, Billerica, MA; #06-570; 1:500 dilution), anti–cyclin B1 (Abcam, Cambridge, MA; #ab72, 1:400 dilution), anti–HK-II (Cell Signaling Technology, Danvers, MA; #2867, 1:100 dilution), and anti–carbonic anhydrase IX (CAIX; Novus Biologicals, Littleton, CO; #NB100-417, 1:500 dilution). This was followed by incubation with HRP polymer conjugate and subsequently with DAB chromogen (SuperPicture Kit; Invitrogen, Camarillo, CA; #87-8963). The sections were counterstained with hematoxylin. Immunohistochemistry for

Ki67 and Glut-1 was performed in the Ventana Benchmark Ultra automated machine. The primary antibodies were anti-Ki67 (Ventana, Tuczon, AZ; #790-4286, 16-minute incubation at 37°C) and anti–Glut-1 (Spring Biosciences, Fremont, CA; #E2840; 1:500 dilution, 24-minute incubation at 37°C). Mounted slides were examined in an Olympus UTV1-X microscope and images were captured with a QImaging Retiga 2000R camera.

Frozen sections were fixed with 4% paraformaldehyde and permeabilized with 0.05% Triton X-100. After blocking with 5% BSA in PBS for 1 hour, the sections were incubated overnight with primary antibodies: rabbit polyclonal anti-CD31 antibody (Abcam; ab28364, 1:50 dilution) or rabbit anti–cleaved caspase-3 antibody (Cell Signaling Technology; 9711s; 1:400) and hypoxia inducible factor-1α (HIF-1α; BD Transduction Laboratory, San Jose, CA), and fluorescein isothiocyanate–conjugated α–smooth muscle actin (SMA; Sigma, St Louis, MO; F3777, 1:500]. The sections were then incubated with secondary antibodies conjugated with Alexa Fluor 488 or Alexa Fluor 594 for 1 hour. Following washing, sections were incubated with 4′,6-diamidino-2-phenylindole (DAPI) and the slides were mounted with Vectashield mounting medium (H1000). The examination of tissue sections were done under a Nikon ECLIPSE Ti series fluorescence microscope, using NIS Elements (BR 3.10) software.

Western Blot

Frozen tissue portions were put in ice-cold lysis buffer and homogenized. The proteins were resolved by sodium dodecyl sulfate–polyacrylamide gel electrophoresis and then transferred onto polyvinylidene difluoride (PVDF) membrane. After blocking for 1 hour with 5% milk in 0.1% Tween 20 in TBS, the membrane was incubated overnight with primary antibodies for HIF-1α (BD Transduction Laboratory; 610958, 1:1000), VEGF (Santa Cruz Biotechnology, Dallas, TX; SC-152, 1:500), and β-actin (Abcam; ab8226, 1:10,000). The membranes were subsequently washed with 0.1% Tween 20 in TBS and incubated with the HRP-conjugated anti-rabbit or anti-mouse secondary (1:10,000) antibodies for 1 hour. The bands were detected by chemiluminescence using Amersham's ECL Plus Western Blot Detection System.

Real-time Polymerase Chain Reaction

Total RNA was extracted from tumor samples using TRIzol reagent (#15596-026; Invitrogen/Life Technologies, Carlsbad, CA) according to the manufacturer's instructions. RNA quality and quantity were determined by gel electrophoresis and spectrophotometry, respectively. Genomic DNA contamination was removed with Deoxyribonuclease I Amplification Grade (#18068-015; Invitrogen/Life Technologies). Synthesis of cDNA was performed using 1 μg of total RNA according to the manufacturer's protocol of ImProm-II Reverse Transcription System (#A3800; Promega, Madison, WI). The primers for PDGF-C and the endogenous gene β-actin (*ACTB*) were designed using Primer Express (3.0) Software from Applied Biosystems (Foster City, CA), taking care that the forward and reverse sequences were in different exons. The sequences of primers for PDGF-C are 5′-GGG CTT GAA GAC CCA GAA GAT-3′ (forward) and 5′-CCA TCA CTG GGT TCC TCA ACT T-3′ (reverse) and those for *ACTB* are 5′-AAGGCCAACCGCGAGAAG-3′ (forward) and 5′-ACAGCCTG-GATAGCAACGTACA-3′ (reverse). Expression levels of PDGF-C was determined by quantitative real-time polymerase chain reaction (PCR). This analysis was performed in a thermocycler Applied Biosystems Prism 7500 Sequence Detection System (PE Applied Biosystems, Inc, Foster City, CA) using relative quantification. The reaction mixture combined 6 μl of SYBR Green PCR Master Mix (#4309155; Applied Biosystems/Life Technologies, Foster City, CA), 3 μl of sense/antisense primers, and 3 μl of cDNA. The cycling conditions were given as follows: 95°C for 10 minutes, 40 cycles of 95°C for 15 seconds, and 60°C for 1 minute. Reactions were done in triplicate. For each sequence, a standard curve was constructed to determine the sensitivity and efficiency assays. For each sample, the cycle threshold (C_t) was determined (mean of the three reactions) for both the target gene and the endogenous control gene and was normalized for cDNA quantity. Subtracting the C_t of the endogenous control gene from the C_t of the target gene yields the ΔC_t. The ΔC_t of the control reference was then subtracted from the ΔC_t of the tumor sample, yielding the $\Delta\Delta C_t$, and the relative quantification value was expressed as $2^{-\Delta\Delta Ct}$.

Statistics

Statistical significance for the difference of mean values for any markers between two treatment groups was assessed by two-tailed *t* test using Graphpad Prism 5.2. For comparing the levels of markers in immunohistochemistry and immunofluorescence experiments, mean pixels indicate the mean readings of four xenografts in each group.

Results

Treatment with TP and PZ

The treatments were started 2 weeks after the subcutaneous injection of tumor cells, when the majority of tumors were 0.5 cm (size range of 0.4-0.7 cm). End points for control, PZ, and TP group tumors were reached after 23, 28, and 46 days (Figure 1), respectively, and tumors were harvested at these times. For TP + PZ, tumor growth was inhibited and remained unchanged until ~50 days, after which they started growing gradually. However, the tumors in TP + PZ–treated animals did not reach the end point until 80 days. Therefore, we were able to examine the effect of continuous treatment with TP + PZ for 28, 56, and 80 days. When the end points were reached or at day 80 (for TP + PZ), the coefficients of variation of tumor sizes

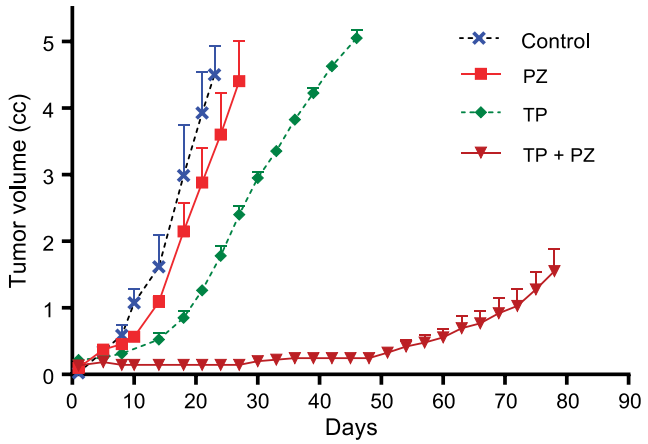

Figure 1. Effect of treatment on tumor growth and survival. The graph represents the effect of treatments on the tumor growth rate. TP + PZ–treated animals did not reach the end point. In the other three groups, all the animals belonging to each group were sacrificed when at least one animal in that group reached the end point.

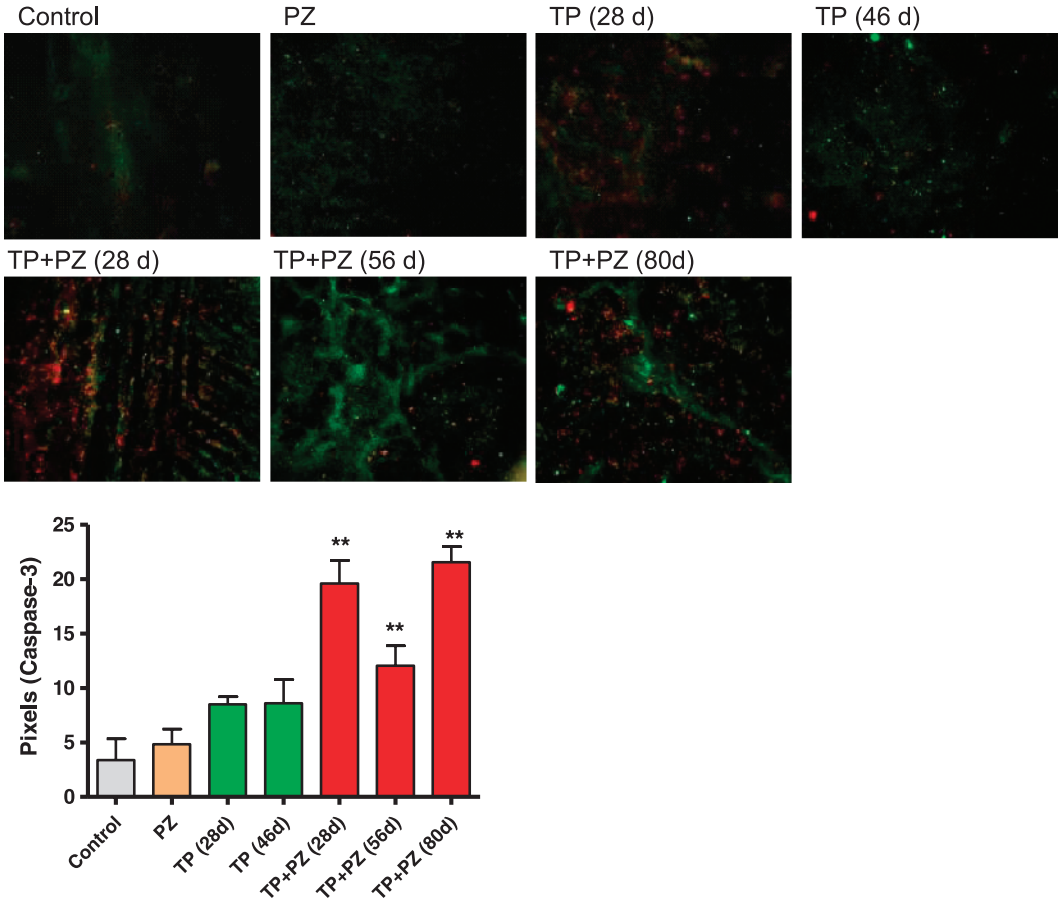

Figure 2. Apoptosis in the tumor tissue after treatment. Microscopic images (magnification, ×20) of tumor sections showing hypoxic areas (HIF-1α positive, green) and cleaved caspase-3 (red). The graph below represents the pixels of caspase-3–stained areas, as measured by ImageJ software.

for control, PZ, TP, and TP + PZ were 0.193, 0.277, 0.049, and 0.301, respectively.

The Effect of Treatments on the Apoptosis, Tumor Hypoxia, and Angiogenic Gene Expression

Immunofluorescence labeling for cleaved caspase-3 (marker of apoptosis) revealed that TP + PZ–treated tumors, at all the three durations, had significantly increased numbers of cleaved caspase-3–positive cells relative to single agents alone (Figure 2). The apoptotic cells were evenly distributed throughout the tumor section rather than being confined to particular areas. Hypoxia marker CAIX [31] showed intensely stained areas for CAIX, observed in the tumors treated with TP for 28 days and those treated with TP + PZ at all three durations (Figure 3*A*). Western blot analysis for HIF-1α revealed intense bands in all treatment groups except for untreated animals and TP-treated animals sacrificed after 46 days of treatment (Figure 3*B*). The tumors treated with TP + PZ for 56 and 80 days showed the highest expression of HIF-1α and VEGF (Figure 3*A*). Real-time PCR revealed that the PDGF-C expression was higher in all the treatment groups, at all durations, compared to the untreated control (Figure 3*C*). It was highest in the later durations (56 and 80 days) of TP + PZ therapy than in other treatment groups. These results highlighted a strong effect of treatment-induced hypoxia likely correlating with an antiangiogenic effect.

The Effect of Treatments on Tumor Vessel Density and Pericyte Coverage

Given the above observations, we next examined the vascularization of these tumors. The markers for endothelial cells and pericytes are CD31 and α-SMA, respectively. Immunofluorescence staining revealed that, compared to the control, none of the single agents at any of the durations reduced the microvessel density, whereas TP + PZ significantly reduced microvessel densities at all the three durations (Figure 4, *A* and *B*). SMA expression increased with time in the TP + PZ group. The mean ratio of SMA to CD31-positive areas was used to compare the extent of pericytic coverage of tumor vasculature (Figure 4*C*). This ratio was significantly higher and ≥1.0 in tumors treated with TP + PZ for 56 and 80 days, while significantly lower in tumors treated with TP + PZ for 28 days, compared to the control tumors. The SMA/CD31 ratio did not vary significantly from control in any of the single agent–treated groups. Control tumors showed both mature blood vessels characterized by larger diameter and thick pericyte coverage (left) and immature blood vessels characterized by smaller diameter and fewer pericyte coverage (right). Although the TP + PZ–treated tumors had higher pericyte coverage, vessels here were smaller than the mature vessels in control tumors. These observations suggested a loss of tumor vascularization but maturation of the remaining few vessels in the TP + PZ tumors.

The Effect of Treatments on Proliferative Index and Mitotic Index of Tumor Cells

The observation that tumor growth was significantly reduced by TP and PZ treatments led us to examine the proliferative and mitotic indices. The number of proliferating cells, as indicated by Ki67 staining, was significantly higher in TP (28 days; $P = .0009$) and TP + PZ (28 days; $P = .0007$) groups relative to the control (Figure 5*A*). However, in all other groups, it did not show a significant difference over control tumors. These contrary results, i.e., stable tumor but with a high proliferative index, indicated a possible cell cycle arrest.

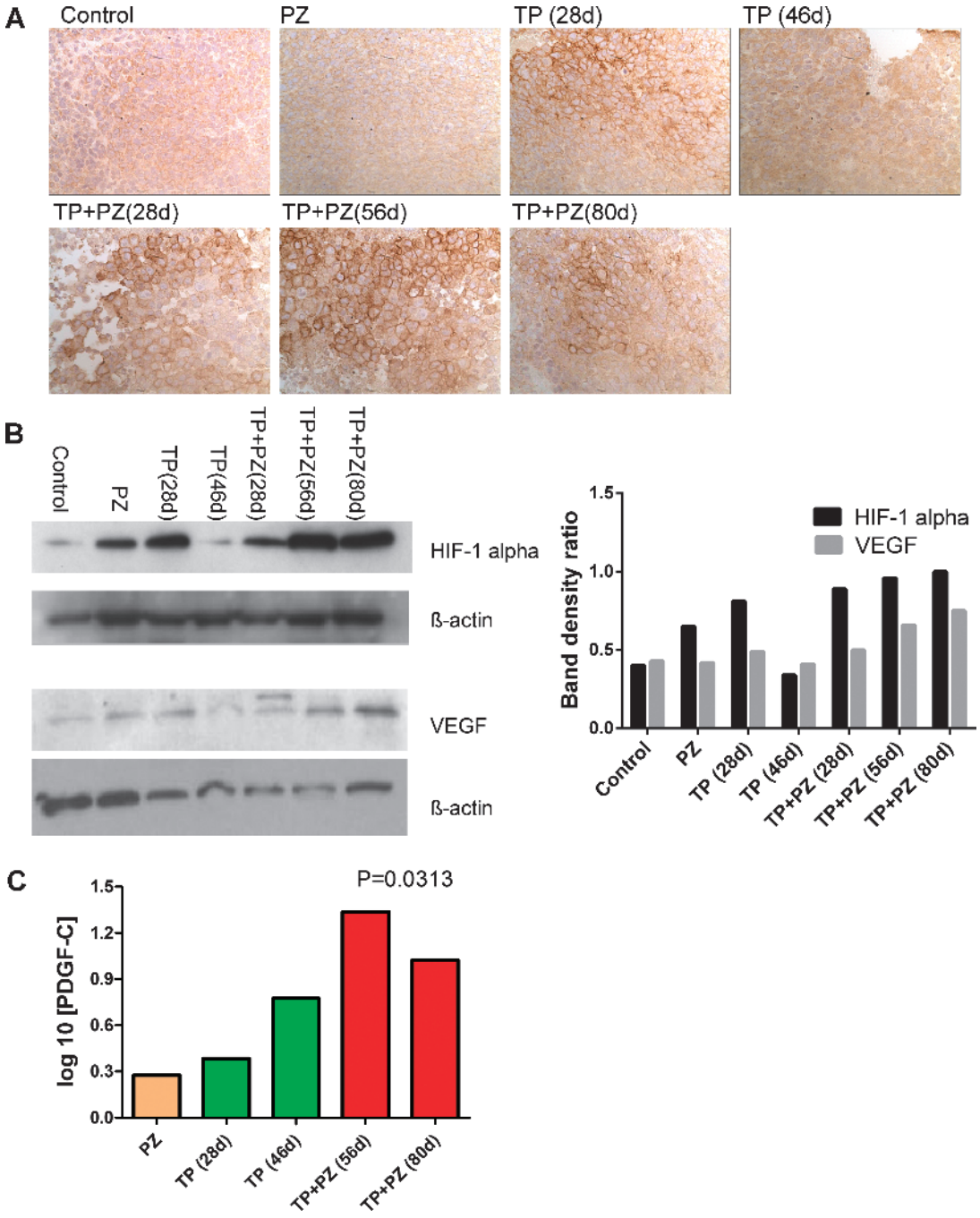

Figure 3. Hypoxia and angiogenic gene expression in tumors after treatment. (A) Microscopic images (magnification, ×40) of tumor sections on which immunohistochemistry for CAIX were performed. (B) Comparison of expression of HIF-1α and VEGF in various treatment groups by Western blot. The band density ratio, which is used as a parameter for comparison of HIF-1α and VEGF expression in the histogram (right), indicates the ratio of band density of HIF-1α or VEGF to that of internal control of that sample. The band density was measured by AlphaEaseFC software. (C) The relative gene expression of PDGF-C with respect to control tumors by $2^{-\Delta\Delta Ct}$ method. The value represents the statistical significance of difference between PDGF-C gene expression in control groups and the mean gene expression in all treatment groups combined. TP + PZ (28 days) was not included because this sample demonstrated RNA degradation (absence of bands for subunits 18 and 28S of RNA by electrophoresis of agarose gel) due to which the C_t value for *ACTB* gene (endogenous gene used in this methodology) was extremely high.

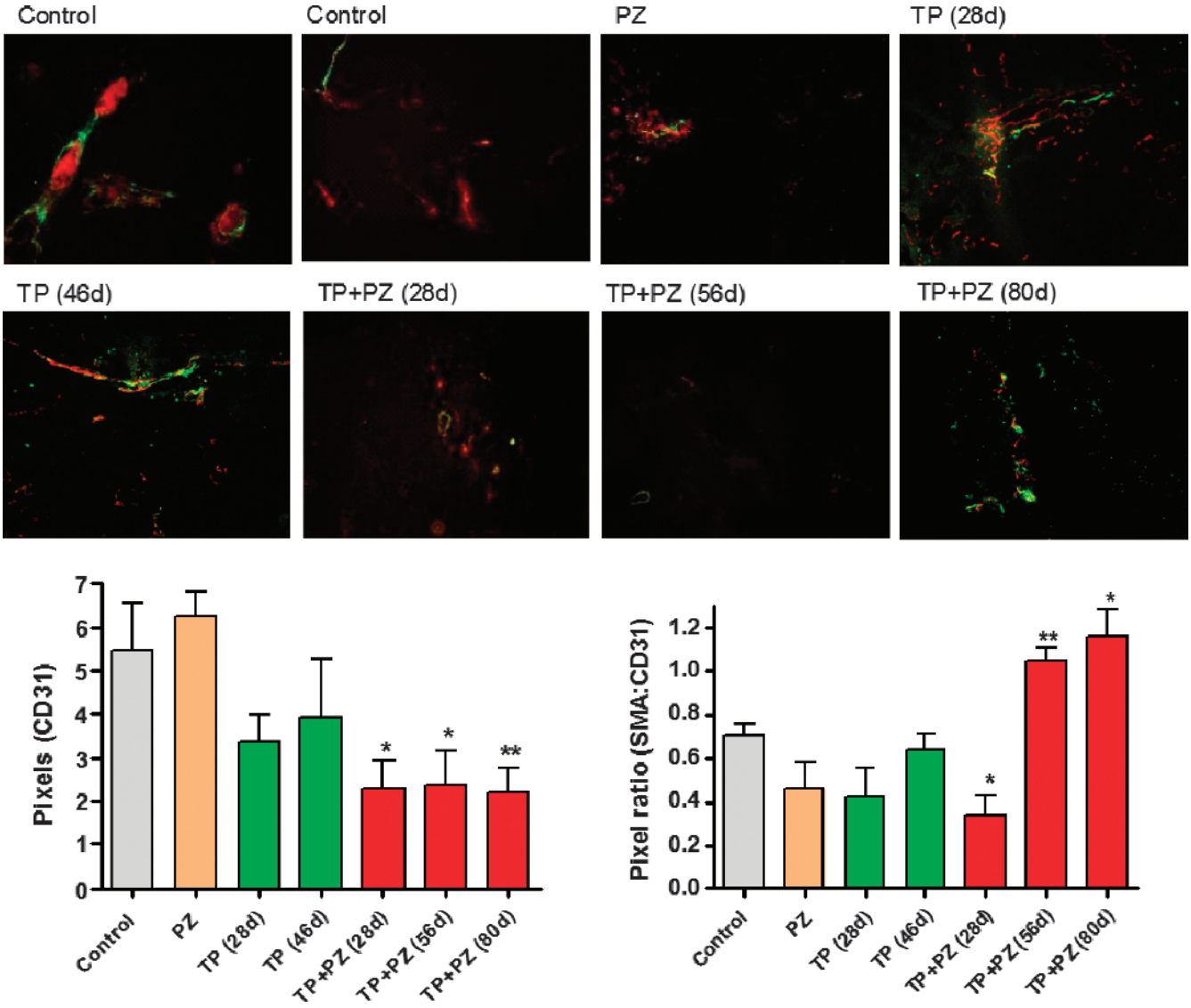

Figure 4. The effect of treatments on tumor vasculature. (Top) Microscopic images (magnification, ×20) of tumor sections showing CD31-positive tumor vasculature (red) and SMA-positive pericytes (green). The two images for control sections indicate the tumor vasculature with a high pericyte coverage (left) and those with low pericyte coverage (right). (Bottom left) The comparison of microvessel densities, measured in terms of pixels of CD31-positive areas in different groups of mice. (Bottom right) The comparison of extent of pericyte coverage, measured in terms of pixel ratio for SMA to CD31-positive areas in different groups of mice. The pixels were measured by ImageJ software.

Therefore, mitotic index of the tumors were measured by PH3 immunohistochemistry. However, compared to control tumors, the mitotic index was significantly higher in TP (28 days; $P = .005$), TP + PZ (28 days; $P = .0002$), and TP + PZ (80 days; $P = .01$) treatment groups (Figure 5*B*).

Effect of Treatments on Glut-1 and HK-II Expression (Indicators of Elevated Glycolysis) by the Tumor Cells

To decipher what could be happening in the tumors as vascularization decreased and remaining vessels stabilized, yet with a more hypoxic microenvironment, we examined other hypoxia and metabolic relevant markers [32]. Immunohistochemistry revealed that expression of Glut-1 and HK-II were significantly higher in the tumors treated with TP + PZ for all three durations, compared to control (Figure 6). In control and single agent–treated tumors, the cells overexpressing Glut-1 were scattered uniformly among those lacking Glut-1 expression. In contrast, in TP + PZ–treated tumors, cells overexpressing Glut-1 were present in groups, separated from those lacking Glut-1 expression.

Discussion

Unlike conventional chemotherapy and therapies that directly targeted tumor cells, antiangiogenic therapy was expected to sustain the antitumor effect because the expected target was genetically stable endothelial cells. However, even antiangiogenic therapy was found to lose efficacy after an initial phase of tumor regression or stabilization. In these cases, resistance mechanisms such as up-regulation of angiogenic factors, vascular maturation, hypoxic adaptation of tumor cells, and enhanced metastatic potential of tumor cells have been reported [33–35]. The molecular evolution of resistant cells

has been studied by proteomic analysis in response to metronomic cyclophosphamide in prostate cancer xenografts, revealing the up-regulation of procoagulant genes and genes conferring reduced dependence on vasculature [36,37]. Conversely, LDM chemotherapy is reported to induce chemosensitivity to endothelial cells as opposed to maximum tolerated dose (MTD), which induces cross-resistance [38]. The residual stem cell population has been reported to be responsible for relapse after metronomic cyclophosphamide in hepatocellular carcinoma xenografts [39]. Prostate cancer cells that acquired resistance to *in vivo* LDM cyclophosphamide has been found to be sensitive to MTD regimen [40].

In our previous preclinical experiments involving LDM topotecan and pazopanib in neuroblastoma, prolonged treatment delayed tumor growth but was unable to stop tumor growth in a neuroblastoma metastatic model [24]. In the present study, we used MYCN-amplified SK-N-BE(2) cell line because MYCN amplification is associated with therapeutic resistance and worse prognosis [41]. Furthermore, as per our experience, SK-N-BE(2) cell line demonstrates uniform growth in experimental mice. Here, the immunofluorescence labeling of the xenografts revealed that tumors treated with TP + PZ maintained a significantly higher level of hypoxia and higher number of apoptotic cells at all the three durations. However, the existing vasculature now exhibited a rich pericyte coverage compared to the control-treated tumors. The cells in tumors treated with TP + PZ for prolonged durations (56 and 80 days) demonstrated comparable or significantly higher proliferative and mitotic indices to that of untreated tumors. However, unlike untreated tumors and other treatment groups, tumors in these 56 and 80 days TP + PZ treatment groups had higher levels of Glut-1 and HK-II, indicative of an adaptation to hypoxia, which could facilitate survival and proliferation under hypoxia.

In the present study, tumor vessel densities in tumors treated with single agents were not significantly different from the control when

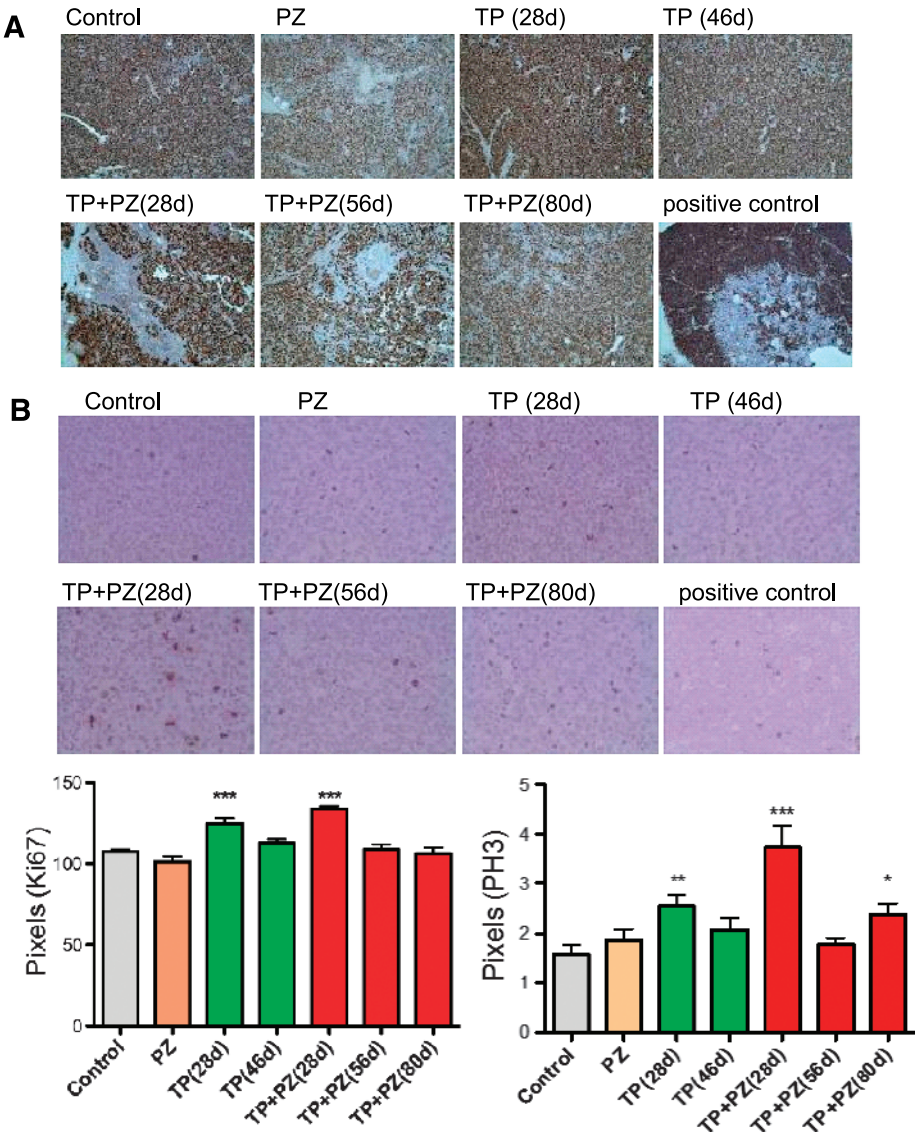

Figure 5. The effect of treatments on proliferation and mitotic index of tumors. Immunohistochemistry on paraffin-embedded tumor sections stained with antibodies for (A) proliferation marker Ki67 (magnification, ×20) and (B) mitotic marker PH3 (magnification, ×40). The brown areas indicate cells or areas expressing Ki67 or PH3. Tonsil was used as positive control for both Ki67 and PH3. The graphs below the images represent the comparison of proliferative and mitotic indices measured as the pixels for areas positive for Ki67 and PH3, respectively.

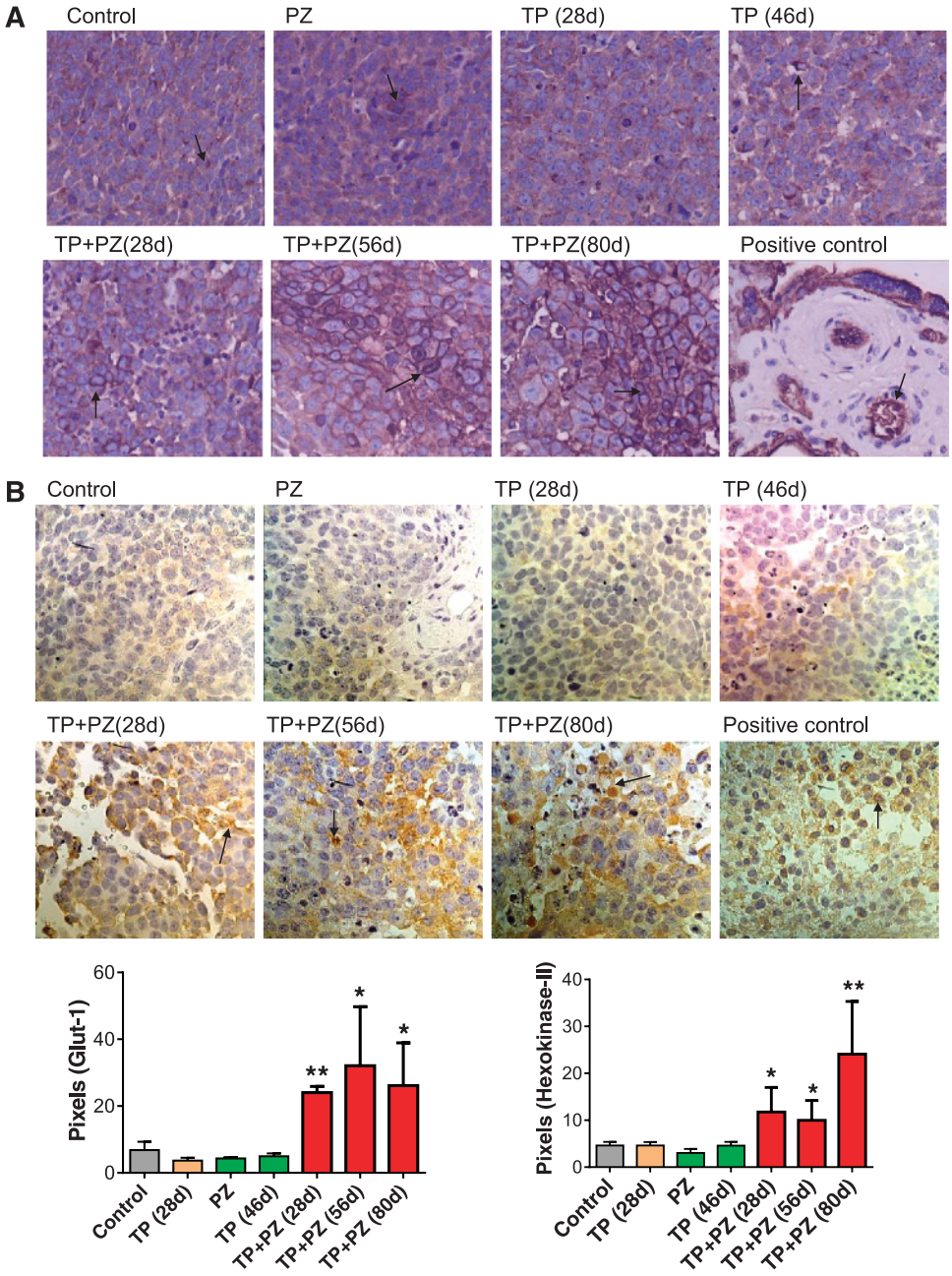

Figure 6. The effect of treatments on markers of aerobic glycolysis. (A) The microscopic images (magnification, ×20) of tissue sections stained for antibody for Glut-1. Placenta was used as positive control tissue. (B) The microscopic images (magnification, ×40) of tissue sections stained with antibody for HK-II. Paraffin-embedded section of a human glioblastoma was used as a positive control. Arrows indicate the cells expressing Glut-1 or HK-II. The histograms below represent the comparison of pixels for Glut-1– or HK-II–stained areas.

they reached the end point. Hence, the loss of efficacy of single agent LDM topotecan and pazopanib can be attributed to the fact that single agents are unable to sustain antiangiogenic effect. Here, angiogenesis may occur due to the expression of factors including VEGF and PDGF-C. In contrast, the tumors in the combination group maintained a low microvessel density even after 56 and 80 days of treatment, the stages when they were growing gradually, despite having higher expressions of VEGF and PDGF-C. Notably, these tumors had higher expression of hypoxia markers HIF-1α and CAIX. Hence, tumors can still acquire resistance by mechanisms other than vascular regrowth. HIF-1α, inducible by hypoxia, is a major cause of antiangiogenic resistance [42]. Our result that TP + PZ upregulates HIF-1α, conflicts with previous reports, where topotecan has been reported to block HIF-1α and reduce VEGF expression in neuroblastoma [43,44]. In addition, combining bevacizumab or sunitinib with low-dose topotecan reduced downstream targets of HIF-1α such as VEGF and Glut-3, simultaneously maintaining a low vessel density in neuroblastoma xenografts [11]. However, in that study, the animals were treated with the combination for only 2 weeks, whereas in our study the earliest sacrifice of animals treated with LDM topotecan and combination was done after 4 weeks (28 days), during which time the tumor phenotype might change. Prolonged observation may be key to revealing phenotypic changes that are informative about the malignant potential.

We entertained the idea that a cause of resistance to the combination therapy could be higher pericyte coverage. Though, in single agent groups, there were pericytes around blood vessels, in the TP + PZ groups treated for 56 and 80 days this fraction was ≥1, indicating that, despite loss of vascularization, all the existing vasculature had pericyte coverage. Tumor vascular maturation characterized by increased pericyte coverage of endothelium is reported to render endothelial cells resistant to apoptotic effects of antiangiogenic therapy [33,34]. PDGF-B and PDGF-C have been implicated in causing vascular maturation [45,46]. PDGF-C has been linked to higher pericyte coverage in glioblastoma. Therefore, our observation of higher PDGF-C expression suggests that PDGF-C may have contributed to the vascular maturation of TP + PZ–treated tumors.

Next, we considered the various mechanisms by which tumors treated with TP + PZ for 56 and 80 days might grow despite the low vasculature and higher hypoxia. This can occur either because of lower apoptosis or higher proliferation rate compared to TP + PZ tumors treated for 28 days. We observed that, although the TP + PZ–treated tumors at all three durations contained a significantly higher number of apoptotic cells, these tumors also had an appreciably higher proliferative index comparable to untreated and single agent–treated tumors. Here, we conclude that although some tumor cells succumbed to antiangiogenic therapy, others had adapted to the hypoxic environment. In stable tumors, the number of apoptotic cells is balanced by proliferating cells. However, in resistant tumors, though the apoptotic cells are significantly higher than those in control group, proliferating cells outnumber these apoptotic cells Another conflicting observation is that tumors treated with TP + PZ for 28 days had a higher proliferative index than any other groups. Considering the stable tumor sizes at this stage of therapy, these tumors would be expected to have relatively lower proliferative indices. Hence, we postulated that this could be an indication of cell cycle arrest. There are reports that cell cycle arrest by therapeutic agents is characterized by dephosphorylation of histone H3, except for the arrest in mitotic phase [47,48]. In our study, however, significantly higher levels of PH3 were observed in TP + PZ–treated tumors after 28 days of treatment, indicating that the number of cells reaching M phase is higher in this group. This then is an indication of a higher proliferative index unless it is mitotic arrest. However, all the reports of hypoxia-induced cell cycle arrest suggests that hypoxia causes cell cycle arrest of cancer cells in G_1 or G_2/M phase [49–51]. There are no reports of hypoxia causing cell cycle arrest in mitotic phase alone. In addition, if direct cytotoxic effect of topotecan on tumor cells is considered, it causes cell cycle arrest before the cells reach mitosis [52]. Therefore, we surmised that the higher Ki67 expression in tumors treated with TP + PZ for 28 days might have indicated a higher proliferative index in this group. On another point, although this could appear improbable, considering the low tumor sizes at this stage of treatment, the possibility is that TP + PZ therapy demonstrated a sustained antiangiogenic efficacy until 80 days. The overall antitumor efficacy achieved by targeting cellular, angiogenic, or immune parameters was lost before 28 days as the tumor cells started to proliferate. Because we do not have TP + PZ tumors collected before 28 days, the actual time limit when TP + PZ therapy could inhibit the proliferation of tumor cells cannot be established by this study. Identifying the actual time of tumor dormancy, i.e., before the tumor cells start proliferating, can be useful in re-inducing tumor dormancy by modifying the therapy at that point.

Our next query was how tumor cells could proliferate in an environment characterized by hypoxia and low vasculature as in the TP + PZ–treated tumors. We postulated that the SK-N-BE(2) tumor xenografts treated with TP + PZ for prolonged durations (56 and 80 days), being comprised of heterogeneous population of cells, included some that were undergoing higher apoptosis and others that had acquired the potential to survive and proliferate under hypoxia. One mechanism by which tumor cells acquire the ability to survive and proliferate under hypoxia is by acquiring dependency on glycolysis, commonly known as the Warburg effect [53,54]. HIF-1α is known to induce the Warburg effect in cancers. Combinatorial effects of MYCN and HIF-1α are reported to promote the proliferation and expression of Glut-1 and HK-II in MYCN-amplified neuroblastoma cells [55]. Glut-1 and HK-II have been used previously as markers of elevated glycolysis [32]. In the Warburg metabolic situation, hypoxic cells compensate for this low output of ATP by increasing the availability of glucose molecules for cellular functions, especially production of metabolites needed for growth. This is where Glut-1, the glucose transporter, plays the pivotal role. Glut-1 is upregulated to facilitate the transport of glucose molecules. Glut-1 up-regulation is associated with an increased proliferation and worse prognosis in neuroblastoma and breast cancers [56,57]. Glut-1 has been proposed to be a marker for hypoxia in solid tumors [31,53,58,59]. Hexokinases are another class of enzymes that catalyze the first step in glycolysis, i.e., phosphorylation of glucose. HK-II is upregulated in cancers to facilitate enhanced glycolysis; therefore, it has been used as a definitive marker of the Warburg effect in many cancers, including neuroblastoma [55,60]. Down-regulation of HK-II in medulloblastoma tumor cells has hampered aerobic glycolysis and reduced the tumorigenic potential in a mouse model [61]. Apart from its role in aerobic glycolysis, HK-II also imparts resistance to chemotherapy-induced apoptosis by binding to the mitochondrial membrane, thereby reducing its permeability [60]. Not surprisingly, clotrimazole, which displaces HK-II from mitochondria, enhances the cytotoxicity of cisplatin in ovarian cancer [62]. The above evidence led us to perform immunohistochemistry for Glut-1 and HK-II in our tumor xenografts. Whereas the control and single agent groups revealed few cells with high Glut-1 expression uniformly scattered within the tumor, TP + PZ–treated tumors had cells showing intense staining for Glut-1 present as clusters. HK-II was also highly expressed in TP + PZ–treated tumors. This indicates that, in this study, TP + PZ–treated tumors become dependent on the glycolytic pathway to meet the energy requirement. We therefore surmise that the hypoxia-challenged tumor cells upregulated HIF-1α that then led to up-regulation of Glut-1 and HK-II, which were needed for resumption of strong tumor growth. Interestingly, we observed foci of such cells suggesting a possible clonogenic effect, that is, outgrowth of hypoxia-resistant clones.

In summary, we report that LDM topotecan and pazopanib, even if used in combination, loses antitumor efficacy after some time. This mechanism of resistance to the combination therapy is different from that to single agent therapy. Whereas the tumors evade antiangiogenic effect of single agent therapy, the combination of these agents demonstrated sustained antiangiogenic effect. The tumors treated with TP + PZ for prolonged duration have a limited but more mature vasculature. Despite sustained antiangiogenic effect, overall antitumor efficacy of TP + PZ is lost because some of the tumor cells acquire capacity to survive and proliferate under antiangiogenesis-induced hypoxia. This in turn drives the glycolytic pathway required for maintenance of tumor growth as revealed by higher staining of Glut-1 and HK-II in TP + PZ–treated tumors. Interestingly, our time study reveals that the tumor cells acquire this capacity long before the tumors start to

show resumption of growth. From a clinical perspective, any sign of a stabilized tumor burden under such treatments should be taken with caution. Instead, further investigations into markers of antiangiogenic resistance would enable clinicians to decide the duration after which the antiangiogenic therapy need to be discontinued or modified. Elevated plasma levels of proangiogenic factors have been suggested as marker of antiangiogenic resistance [63]. On the basis of the present study, we also suggest that indicators of proliferation, cell cycle, and elevated glycolysis in circulating tumor cells can be potential biomarkers of antiangiogenic resistance. Furthermore, the contrary results between this study and previous short-term studies, with respect to HIF-1α and downstream targets in neuroblastoma, supports the need for long-term preclinical investigation of antiangiogenic therapies if they are to be considered as maintenance regimen [11]. In effect, combining antiangiogenic therapies with drugs targeting tumor metabolism could be a more effective strategy to overcome antiangiogenic resistance [42].

Acknowledgments

Tissue section preparation and immunohistochemistry for Ki67 and Glut-1 using Ventana automated instrument were performed by Pathology Research Laboratory, Department of Pediatric Laboratory Medicine, The Hospital for Sick Children.

References

[1] Smith MA, Seibel NL, Altekruse SF, Ries LA, Melbert DL, O'Leary M, Smith FO, and Reaman GH (2010). Outcomes for children and adolescents with cancer: challenges for the twenty-first century. *J Clin Oncol* **28**, 2625–2634.

[2] SEER (2003). Surveillance, epidemiology, and end results (SEER) program web site. Available at http://www.seer.cancer.gov.

[3] Taylor M, Rössler J, Geoerger B, Vassal G, and Farace F (2010). New anti-angiogenic strategies in pediatric solid malignancies: agents and biomarkers of a near future. *Expert Opin Investig Drugs* **19**, 859–874.

[4] Kerbel RS and Kamen BA (2004). The anti-angiogenic basis of metronomic chemotherapy. *Nat Rev Cancer* **4**, 423–436.

[5] Stempak D, Seely D, and Baruchel S (2006). Metronomic dosing of chemotherapy: applications in pediatric oncology. *Cancer Invest* **24**, 432–443.

[6] Hackl C, Man S, Francia G, Milsom C, Xu P, and Kerbel RS (2013). Metronomic oral topotecan prolongs survival and reduces liver metastasis in improved preclinical orthotopic and adjuvant therapy colon cancer models. *Gut* **62**, 259–271.

[7] Pasquier E, Kavallaris M, and André N (2010). Metronomic chemotherapy: new rationale for new directions. *Nat Rev Clin Oncol* **7**, 455–465.

[8] Wei J, DeAngulo G, Sun W, Hussain SF, Vasquez H, Jordan J, Weinberg J, Wolff J, Koshkina N, and Heimberger AB (2009). Topotecan enhances immune clearance of gliomas. *Cancer Immunol Immunother* **58**, 259–270.

[9] Galluzzi L, Senovilla L, Zitvogel L, and Kroemer G (2012). The secret ally: immunostimulation by anticancer drugs. *Nat Rev Drug Discov* **3**, 215–233.

[10] Klement G, Baruchel S, Rak J, Man S, Clark K, Hicklin DJ, Bohlen P, and Kerbel RS (2000). Continuous low-dose therapy with vinblastine and VEGF receptor-2 antibody induces sustained tumor regression without overt toxicity. *J Clin Invest* **105**, R15–R24.

[11] Hartwich J, Orr WS, Ng CY, Spence Y, Morton C, and Davidoff AM (2013). HIF-1α activation mediates resistance to anti-angiogenic therapy in neuroblastoma xenografts. *J Pediatr Surg* **48**, 39–46.

[12] Tran Cao HS, Bouvet M, Kaushal S, Keleman A, Romney E, Kim G, Fruehauf J, Imagawa DK, Hoffman RM, and Katz MH (2010). Metronomic gemcitabine in combination with sunitinib inhibits multisite metastasis and increases survival in an orthotopic model of pancreatic cancer. *Mol Cancer Ther* **9**, 2068–2078.

[13] Jia L and Waxman DJ (2013). Thrombospondin-1 and pigment epithelium-derived factor enhance responsiveness of KM12 colon tumor to metronomic cyclophosphamide but have disparate effects on tumor metastasis. *Cancer Lett* **330**, 241–249.

[14] Wang R, Qin S, Chen Y, Li Y, Chen C, Wang Z, Zheng R, and Wu Q (2012). Enhanced anti-tumor and anti-angiogenic effects of metronomic cyclophosphamide combined with Endostar in a xenograft model of human lung cancer. *Oncol Rep* **28**, 439–445.

[15] Eichbaum M, Mayer C, Eickhoff R, Bischofs E, Gebauer G, Fehm T, Lenz F, Fricke HC, Solomayer E, Fersis N, et al. (2011). The PACOVAR-trial: a phase I/II study of pazopanib (GW786034) and cyclophosphamide in patients with platinum-resistant recurrent, pre-treated ovarian cancer. *BMC Cancer* **20**, 453.

[16] Dellapasqua S, Bertolini F, Bagnardi V, Campagnoli E, Scarano E, Torrisi R, Shaked Y, Mancuso P, Goldhirsch A, Rocca A, et al. (2008). Metronomic cyclophosphamide and capecitabine combined with bevacizumab in advanced breast cancer. *J Clin Oncol* **26**, 4899–4905.

[17] Montagna E, Cancello G, Bagnardi V, Pastrello D, Dellapasqua S, Perri G, Viale G, Veronesi P, Luini A, Intra M, et al. (2012). Metronomic chemotherapy combined with bevacizumab and erlotinib in patients with metastatic HER2-negative breast cancer: clinical and biological activity. *Clin Breast Cancer* **12**, 207–214.

[18] Garcia AA, Hirte H, Fleming G, Yang D, Tsao-Wei DD, Roman L, Groshen S, Swenson S, Markland F, Gandara D, et al. (2008). Phase II clinical trial of bevacizumab and low-dose metronomic oral cyclophosphamide in recurrent ovarian cancer: a trial of the California, Chicago, and Princess Margaret Hospital phase II consortia. *J Clin Oncol* **26**, 76–82.

[19] Stempak D, Gammon J, Halton J, Moghrabi A, Koren G, and Baruchel S (2006). A pilot pharmacokinetic and antiangiogenic biomarker study of celecoxib and low-dose metronomic vinblastine or cyclophosphamide in pediatric recurrent solid tumors. *J Pediatr Hematol Oncol* **28**, 720–728.

[20] Felgenhauer JL, Nieder ML, Krailo MD, Bernstein ML, Henry DW, Malkin D, Baruchel S, Chuba PJ, Sailer SL, Brown K, et al. (2013). A pilot study of low-dose anti-angiogenic chemotherapy in combination with standard multi-agent chemotherapy for patients with newly diagnosed metastatic Ewing sarcoma family of tumors: a Children's Oncology Group (COG) phase II study NCT00061893. *Pediatr Blood Cancer* **60**, 409–414.

[21] Pasquier E, Kieran MW, Sterba J, Shaked Y, Baruchel S, Oberlin O, Kivivuori MS, Peyrl A, Diawarra M, Casanova M, et al. (2011). Moving forward with metronomic chemotherapy: meeting report of the 2nd International Workshop on Metronomic and Anti-Angiogenic Chemotherapy in Paediatric Oncology. *Transl Oncol* **4**, 203–211.

[22] Hashimoto K, Man S, Xu P, Cruz-Munoz W, Tang T, Kumar R, and Kerbel RS (2010). Potent preclinical impact of metronomic low-dose oral topotecan combined with the antiangiogenic drug pazopanib for the treatment of ovarian cancer. *Mol Cancer Ther* **9**, 996–1006.

[23] Merritt WM, Nick AM, Carroll AR, Lu C, Matsuo K, Dumble M, Jennings N, Zhang S, Lin YG, Spannuth WA, et al. (2010). Bridging the gap between cytotoxic and biologic therapy with metronomic topotecan and pazopanib in ovarian cancer. *Mol Cancer Ther* **9**, 985–995.

[24] Kumar S, Mokhtari RB, Sheikh R, Wu B, Zhang L, Xu P, Man S, Oliveira ID, Yeger H, Kerbel RS, et al. (2011). Metronomic oral topotecan with pazopanib is an active antiangiogenic regimen in mouse models of aggressive pediatric solid tumor. *Clin Cancer Res* **17**, 5656–5667.

[25] Tillmanns TD, Reed ME, Privett MC, Johns AL, Walker MS, and Houts AC (2012). Phase I trial of metronomic oral topotecan in combination with pazopanib utilizing a daily dosing schedule to treat recurrent or persistent gynecologic tumors. In *Proceedings of American Society for Clinical Oncology Annual Meeting (ASCO), Chicago, IL*. Abstract #5014.

[26] Kesari S, Schiff D, Doherty L, Gigas DC, Batchelor TT, Muzikansky A, O'Neill A, Drappatz J, Chen-Plotkin AS, Ramakrishna N, et al. (2007). Phase II study of metronomic chemotherapy for recurrent malignant gliomas in adults. *Neuro Oncol* **9**, 354–363.

[27] Verhoeff JJ, van Tellingen O, Claes A, Stalpers LJ, van Linde ME, Richel DJ, Leenders WP, and van Furth WR (2009). Concerns about anti-angiogenic treatment in patients with glioblastoma multiforme. *BMC Cancer* **9**, 444.

[28] Reardon DA, Desjardins A, Vredenburgh JJ, Gururangan S, Sampson JH, Sathornsumetee S, McLendon RE, Herndon JE II, Marcello JE, Norfleet J, et al. (2009). Metronomic chemotherapy with daily, oral etoposide plus bevacizumab for recurrent malignant glioma: a phase II study. *Br J Cancer* **101**, 1986–1994.

[29] Reardon DA, Desjardins A, Peters K, Gururangan S, Sampson J, Rich JN, McLendon R, Herndon JE II, Marcello J, Threatt S, et al. (2011). Phase II study of metronomic chemotherapy with bevacizumab for recurrent glioblastoma after progression on bevacizumab therapy. *J Neurooncol* **103**, 371–379.

[30] Tamaskar I, Dhillon J, and Pili R (2011). Resistance to angiogenesis inhibitors in renal cell carcinoma. *Clin Adv Hematol Oncol* **9**, 101–110.

[31] Sørensen BS, Hao J, Overgaard J, Alsner J, and Horsman MR (2005). Validating the use of CAIX and GLUT1 as endogenous markers for hypoxia in solid tumors. In *Proceedings of 96th Annual Meeting of the American Association for Cancer Research (AACR), Anaheim, CA*. Abstract #1130.

[32] Milane L, Duan Z, and Amiji M (2011). Role of hypoxia and glycolysis in the development of multi-drug resistance in human tumor cells and the establishment of an orthotopic multi-drug resistant tumor model in nude mice using hypoxic pre-conditioning. *Cancer Cell Int* **11**, 3.

[33] Bergers G and Hanahan D (2008). Modes of resistance to anti-angiogenic therapy. *Nat Rev Cancer* **8**, 592–603.

[34] Loges S, Schmidt T, and Carmeliet P (2010). Mechanisms of resistance to anti-angiogenic therapy and development of third-generation anti-angiogenic drug candidates. *Genes Cancer* **1**, 12–25.

[35] Yu JL, Rak JW, Coomber BL, Hicklin DJ, and Kerbel RS (2002). Effect of p53 status on tumor response to antiangiogenic therapy. *Science* **295**, 1526–1528.

[36] Thoenes L, Hoehn M, Kashirin R, Ogris M, Arnold GJ, Wagner E, and Guenther M (2010). *In vivo* chemoresistance of prostate cancer in metronomic cyclophosphamide therapy. *J Proteomics* **73**, 1342–1354.

[37] Kubisch R, Meissner L, Krebs S, Blum H, Günther M, Roidl A, and Wagner E (2013). A comprehensive gene expression analysis of resistance formation upon metronomic cyclophosphamide therapy. *Transl Oncol* **6**, 1–9.

[38] Pasquier E, Tuset MP, Street J, Sinnappan S, Mackenzie KL, Braguer D, Andre N, and Kavallaris M (2013). Concentration- and schedule-dependent effects of chemotherapy on the angiogenic potential and drug sensitivity of vascular endothelial cells. *Angiogenesis* **16**, 373–386.

[39] Martin-Padura I, Marighetti P, Agliano A, Colombo F, Larzabal L, Redrado M, Bleau AM, Prior C, Bertolini F, and Calvo A (2012). Residual dormant cancer stem-cell foci are responsible for tumor relapse after antiangiogenic metronomic therapy in hepatocellular carcinoma xenografts. *Lab Invest* **92**, 952–966.

[40] Emmenegger U, Francia G, Chow A, Shaked Y, Kouri A, Man S, and Kerbel RS (2011). Tumors that acquire resistance to low-dose metronomic cyclophosphamide retain sensitivity to maximum tolerated dose cyclophosphamide. *Neoplasia* **13**, 40–48.

[41] Veas-Perez de Tudela M, Delgado-Esteban M, Cuende J, Bolaños JP, and Almeida A (2010). Human neuroblastoma cells with MYCN amplification are selectively resistant to oxidative stress by transcriptionally up-regulating glutamate cysteine ligase. *J Neurochem* **113**, 819–825.

[42] Rapisarda A and Melillo G (2012). Overcoming disappointing results with anti-angiogenic therapy by targeting hypoxia. *Nat Rev Clin Oncol* **9**, 378–390.

[43] Puppo M, Battaglia F, Ottaviano C, Delfino S, Ribatti D, Varesio L, and Bosco MC (2008). Topotecan inhibits vascular endothelial growth factor production and angiogenic activity induced by hypoxia in human neuroblastoma by targeting hypoxia-inducible factor-1α and -2α. *Mol Cancer Ther* **7**, 1974–1984.

[44] Beppu K, Nakamura K, Linehan WM, Rapisarda A, and Thiele CJ (2005). Topotecan blocks hypoxia-inducible factor-1α and vascular endothelial growth factor expression induced by insulin-like growth factor-I in neuroblastoma cells. *Cancer Res* **65**, 4775–4781.

[45] di Tomaso E, London N, Fuja D, Logie J, Tyrrell JA, Kamoun W, Munn LL, and Jain RK (2009). PDGF-C induces maturation of blood vessels in a model of glioblastoma and attenuates the response to anti-VEGF treatment. *PLoS One* **4**, e5123.

[46] Abramsson A, Lindblom P, and Betsholtz C (2003). Endothelial and non-endothelial sources of PDGF-B regulate pericyte recruitment and influence vascular pattern formation in tumors. *J Clin Invest* **112**, 1142–1151.

[47] Liu CY, Chang HS, Chen IS, Chen CJ, Hsu ML, Fu SL, and Chen YJ (2011). Costunolide causes mitotic arrest and enhances radiosensitivity in human hepatocellular carcinoma cells. *Radiat Oncol* **6**, 56.

[48] Lee CC, Lin YH, Chang WH, Lin PC, Wu YC, and Chang JG (2011). Squamocin modulates histone H3 phosphorylation levels and induces G_1 phase arrest and apoptosis in cancer cells. *BMC Cancer* **11**, 58.

[49] Box AH and Demetrick DJ (2004). Cell cycle kinase inhibitor expression and hypoxia-induced cell cycle arrest in human cancer cell lines. *Carcinogenesis* **25**, 2325–2335.

[50] Manohar SM, Padgaonkar AA, Jalota-Badhwar A, Rao SV, and Joshi KS (2012). Cyclin-dependent kinase inhibitor, P276-00, inhibits HIF-1α and induces G2/M arrest under hypoxia in prostate cancer cells. *Prostate Cancer Prostatic Dis* **15**, 15–27.

[51] Lou J, Zhou X, Weng Q, Wang DD, Xia Q, Hu Y, He Q, Yang B, and Luo P (2010). XQ2, a novel TPZ derivative, induced G2/M phase arrest and apoptosis under hypoxia in non-small cell lung cancer cells. *Biosci Biotechnol Biochem* **74**, 1181–1187.

[52] Feeney GP, Errington RJ, Wiltshire M, Marquez N, Chappell SC, and Smith PJ (2003). Tracking the cell cycle origins for escape from topotecan action by breast cancer cells. *Br J Cancer* **88**, 1310–1317.

[53] Airley R, Loncaster J, Davidson S, Bromley M, Roberts S, Patterson A, Hunter R, Stratford I, and West C (2001). Glucose transporter Glut-1 expression correlates with tumor hypoxia and predicts metastasis-free survival in advanced carcinoma of the cervix. *Clin Cancer Res* **7**, 928–934.

[54] Vander Heiden MG, Cantley LC, and Thompson CB (2009). Understanding the Warburg effect: the metabolic requirements of cell proliferation. *Science* **324**, 1029–1033.

[55] Qing G, Skuli N, Mayes PA, Pawel B, Martinez D, Maris JM, and Simon MC (2010). Combinatorial regulation of neuroblastoma tumor progression by N-Myc and hypoxia inducible factor HIF-1α. *Cancer Res* **70**, 10351–10361.

[56] Matsushita K, Uchida K, Saigusa S, Ide S, Hashimoto K, Koike Y, Otake K, Inoue M, Tanaka K, and Kusunoki M (2012). Glycolysis inhibitors as a potential therapeutic option to treat aggressive neuroblastoma expressing GLUT1. *J Pediatr Surg* **47**, 1323–1330.

[57] Kang SS, Chun YK, Hur MH, Lee HK, Kim YJ, Hong SR, Lee JH, Lee SG, and Park YK (2002). Clinical significance of glucose transporter 1 (GLUT1) expression in human breast carcinoma. *Jpn J Cancer Res* **93**, 1123–1128.

[58] Chung FY, Huang MY, Yeh CS, Chang HJ, Cheng TL, Yen LC, Wang JY, and Lin SR (2009). GLUT1 gene is a potential hypoxic marker in colorectal cancer patients. *BMC Cancer* **9**, 241.

[59] Rademakers SE, Lok J, van der Kogel AJ, Bussink J, and Kaanders JH (2011). Metabolic markers in relation to hypoxia; staining patterns and colocalization of pimonidazole, HIF-1α, CAIX, LDH-5, GLUT-1, MCT1 and MCT4. *BMC Cancer* **11**, 167.

[60] Mathupala SP, Ko YH, and Pedersen PL (2006). Hexokinase II: cancer's double-edged sword acting as both facilitator and gatekeeper of malignancy when bound to mitochondria. *Oncogene* **25**, 4777–4786.

[61] Gershon RT, Crowther AJ, Tikunov A, Garcia I, Annis R, Yuan H, Miller CR, Macdonald J, Olson J, and Deshmukh M (2013). Hexokinase-2-mediated aerobic glycolysis is integral to cerebellar neurogenesis and pathogenesis of medulloblastoma. *Cancer Metab* **1**, 2.

[62] Shulga N, Wilson-Smith R, and Pastorino JG (2009). Hexokinase II detachment from the mitochondria potentiates cisplatin induced cytotoxicity through a caspase-2 dependent mechanism. *Cell Cycle* **8**, 3355–3364.

[63] Jain RK, Duda DG, Willett CG, Sahani DV, Zhu AX, Loeffler JS, Batchelor TT, and Sorensen AG (2009). Biomarkers of response and resistance to anti-angiogenic therapy. *Nat Rev Clin Oncol* **6**, 327–338.